How Kondo-holes create intense nanoscale heavy-fermion hybridization disorder

Mohammad H. Hamidian[a,b,1], Andrew R. Schmidt[a,b,c,1], Inês A. Firmo[a,b], Milan P. Allan[a,d], Phelim Bradley[e], Jim D. Garrett[f], Travis J. Williams[g], Graeme M. Luke[g,h], Yonatan Dubi[i,j], Alexander V. Balatsky[i], and J. C. Davis[a,b,d,k,2]

[a]Department of Physics, Laboratory for Atomic and Solid State Physics, Cornell University, Ithaca, NY 14853; [b]Condensed Matter Physics and Materials Science Department, Brookhaven National Laboratory, Upton, NY 11973; [c]Department of Physics, University of California, Berkeley, CA 94720; [d]Scottish Universities Physics Alliance (SUPA), School of Physics and Astronomy, University of Saint Andrews, North Haugh, Saint Andrews KY16 9SS, United Kingdom; [e]Department of Physics, University College Cork, County Cork, Ireland; [f]Brockhouse Institute for Materials Research, McMaster University, Hamilton, ON, Canada L8S 4M1; [g]Department of Physics and Astronomy, McMaster University, Hamilton, ON, Canada L8S 4M1; [h]Canadian Institute for Advanced Research, Toronto, ON, Canada M5G 1Z8; [i]Theory Division, Los Alamos National Lab, Los Alamos, NM 87545; [j]Sackler School of Physics and Astronomy, Tel Aviv University, Tel Aviv 69978, Israel; and [k]Kavli Institute at Cornell for Nanoscale Science, Cornell University, Ithaca, NY 14850

Contributed by J.C. Séamus Davis, September 13, 2011 (sent for review July 27, 2011)

Replacing a magnetic atom by a spinless atom in a heavy-fermion compound generates a quantum state often referred to as a "Kondo-hole". No experimental imaging has been achieved of the atomic-scale electronic structure of a Kondo-hole, or of their destructive impact [Lawrence JM, et al. (1996) *Phys Rev B* 53:12559–12562] [Bauer ED, et al. (2011) *Proc Natl Acad Sci.* 108:6857–6861] on the hybridization process between conduction and localized electrons which generates the heavy-fermion state. Here we report visualization of the electronic structure at Kondo-holes created by substituting spinless thorium atoms for magnetic uranium atoms in the heavy-fermion system URu_2Si_2. At each thorium atom, an electronic bound state is observed. Moreover, surrounding each thorium atom we find the unusual modulations of hybridization strength recently predicted to occur at Kondo-holes [Figgins J, Morr DK (2011) *Phys Rev Lett* 107:066401]. Then, by introducing the "hybridization gapmap" technique to heavy-fermion studies, we discover intense nanoscale heterogeneity of hybridization due to a combination of the randomness of Kondo-hole sites and the long-range nature of the hybridization oscillations. These observations provide direct insight into both the microscopic processes of heavy-fermion forming hybridization and the macroscopic effects of Kondo-hole doping.

Kondo lattice | spectroscopic imaging STM | correlated electrons | QPI

Kondo Lattice Generated Heavy Fermions

Within a Kondo lattice (Fig. 1*A*), an f-electron state localized at each magnetic atom becomes hybridized at low temperatures with the delocalized conduction electrons of the metal (1–4). The resulting "heavy-fermion" electronic structure in momentum space (**k**-space) is shown schematically in Fig. 1*B*. Here the original light conduction band $\varepsilon^c(\mathbf{k})$ splits into two distinct heavy bands within an energy range often referred to as the direct (4) "hybridization gap" Δ_h (Fig. 1 *B* and *C*). This energy range is determined by the strength of the matrix element $V_h(\approx\Delta_h/2)$ for the quantum conversion of a conduction electron into an f-electron and vice versa, and (in simplest models) is not centered on the Fermi energy but on the renormalized energy level of the localized f-electron ε^f (Fig. 1 *B* and *C* and refs. 2–4). The value of Δ_h is defined quantitatively (2–6) in **k**-space as the energy-separation between the heavy-fermion bands at the wavevector $\mathbf{k}^c(\varepsilon^f)$ where ε^f intersects the light conduction band (Fig. 1*B*), and equivalently in real-space (**r**-space) as the energy range within which changes occur in the density-of-states due to appearance of the heavy-fermion bands (Fig. 1*C*). We note that Δ_h is not the energy gap of a symmetry-breaking electronic phase transition, but merely the energy range of a quantum mechanical avoided crossing in **k**-space (Fig. 1 *B* and *C*). Very recently it has become possible to detect both the characteristic **k**-space (7) and **r**-space (8) signatures of this heavy-fermion hybridization gap by using spectroscopic imaging scanning tunneling microscopy (SI-STM), with the observations being in excellent agreement with theoretical expectations.

Kondo Resonances and Kondo-Holes

Heavy-fermions owe their existence to a special quantum mechanical many-body state that appears at a magnetic rare earth or actinide atom when embedded in a metal. The atom's magnetic moment is screened by the formation of a spin-zero many-body electronic state (1–4), often referred to as the "Kondo resonance" (blue atom Fig. 2*A*). Kondo resonances have been imaged directly at individual magnetic adatoms on metal surfaces (9–11) by using SI-STM to map the differential tunneling conductance $dI/dV(\mathbf{r},\varepsilon = ev) \equiv g(\mathbf{r},\varepsilon) \propto N(\mathbf{r},\varepsilon)$. Here v is the tip-sample bias voltage for electron tunneling and $N(\mathbf{r},\varepsilon)$ is the electronic density-of-states. A distinct type of many-body state, which can be considered dual to the Kondo resonance, occurs when a single nonmagnetic atom is substituted within the array of otherwise magnetic atoms of a heavy-fermion system (green atom Fig. 2*B*). This state is often referred to as a "Kondo-hole". Although experimentally there is good understanding of the electronic structure at individual Kondo resonances (9–11), the atomic-scale electronic phenomena surrounding Kondo-holes have remained unexplored.

Electronic Structure of a Kondo-Hole

Understanding the electronic structure of a Kondo-hole is of fundamental and practical consequence to the study of rare earth and actinide heavy-fermion metals and superconductors. In such studies, the classic experimental approach is to determine the macroscopic response to random Kondo-hole doping (12–18). A wide variety of key issues in heavy-fermion physics have been studied this way including: (*i*) dilution and the resulting nanoscale spatial heterogeneity in the hybridization process (12–14, 18); (*ii*) the local perturbations to the hybridization and heavy-fermion formation at individual Kondo-holes (14, 17, 18); (*iii*) local impurity states bound within the hybridization gap at the Kondo-hole, and their impact on scattering (12–15, 17); (*iv*) the temperature minimum in resistivity possibly due to the special scattering properties of states bound within the doped Kondo-holes (14–17); (*v*) the impact of Kondo-holes on the development of

Author contributions: M.H.H., A.R.S., and J.C.D. designed research; M.H.H., A.R.S., J.D.G., T.J.W., and G.M.L. performed research; J.D.G., T.J.W., and G.M.L. synthesized samples; M.H.H., A.R.S., I.A.F., M.P.A., P.B., Y.D., and A.V.B. analyzed data; and J.C.D. wrote the paper.

The authors declare no conflict of interest.

See Commentary on page 18191.

[1]M.H.H. and A.R.S. contributed equally to this work.

[2]To whom correspondence should be addressed. E-mail: jcdavis@ccmr.cornell.edu.

This article contains supporting information online at www.pnas.org/lookup/suppl/doi:10.1073/pnas.1115027108/-/DCSupplemental.

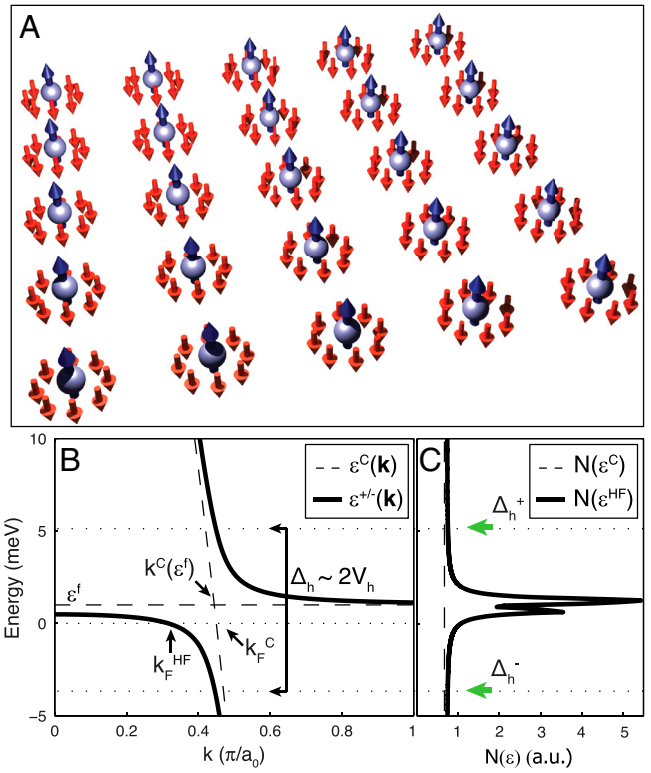

Fig. 1. Schematic of the **r**-space and **k**-space electronic structure of a simple heavy-fermion system. (*A*) Schematic of a Kondo lattice. The atoms/spins shown in blue represent the magnetic atoms. The conduction electrons which screen these moments at low temperature are indicated schematically in red. (*B*) Schematic of a simple heavy-fermion band structure in **k**-space. Here the (light) conduction electron band $\varepsilon^c(\mathbf{k})$ is hole-like and indicated by the steeply sloping dashed line. The two heavy-fermion bands are indicated by solid lines, with the energy range of their avoided crossing, the hybridization gap Δ_h, as shown. (*C*) Schematic of the density-of-states $N(\varepsilon)$ simulated at finite temperature for a heavy-fermion system as shown in (*B*). We see clearly how Δ_h can be determined in **r**-space by identifying the energy range between $\Delta_h(\mathbf{r}) = \Delta_h^+(\mathbf{r}) - \Delta_h^-(\mathbf{r})$ within which the $N(\varepsilon)$ is perturbed from its structure before the heavy-fermion bands appeared.

coherence in the heavy-fermion band (12, 14, 15, 17, 18); and (*vi*) how Kondo-holes destroy unconventional superconductivity due to their special pair-breaking scattering (12–14, 16–18). While the macroscopic effects of nonmagnetic dopant atoms are evident throughout these studies, knowledge of the microscopic electronic phenomenology of individual Kondo-holes, and precisely how they disorder the hybridization process producing the heavy-fermions, could greatly improve the precision and significance of the resulting conclusions.

Kondo-Hole Theory

Theoretical predictions for the impact of Kondo-holes on the surrounding electronic structure and on the hybridization process generating the heavy-fermions include that: (*i*) increasing densities of Kondo-holes will progressively degrade hybridization and its related effects on $N(\varepsilon)$ in a heterogeneous fashion at nanoscale (19–21)—eventually destroying the heavy-fermion state; (*ii*) a special bound impurity state should exist within the hybridization gap at each Kondo-hole site (20–22); (*iii*) the electrical resistivity should exhibit a minimum and then increase with falling T because of the unique scattering properties of these bound states (19–21); and (*iv*) the heavy-fermion superconductivity in non s-wave systems should be strongly suppressed by pair-breaking scattering at each Kondo-hole (23). More recent modelling of electronic structure surrounding a single Kondo-hole analyzes the atomic-scale variations in hybridization strength $V(\mathbf{r})$, the density-of-states $N(\mathbf{r},\varepsilon)$, and the electronic impurity state bound inside the altered hybridization gap (22). Fig. 2*C* shows the prediction for modulations in the strength of hybridization surrounding a Kondo-hole (22) with the key observation being that $V_h(\propto \Delta_h(\mathbf{r}))$ oscillates with wavevector $\mathbf{Q}^* \cong 2\mathbf{k}_F^c$, twice the Fermi wavevector of the original light (unhybridized) conduction band (Fig. 2*D*). Such hybridization oscillations would be quite distinct from the heavy-fermion Friedel oscillations in $N(\mathbf{r},\varepsilon = 0)$ which have been observed at $\mathbf{q} = 2\mathbf{k}_F^{HF}$ (7), where $\mathbf{k}_F^{HF}$ is the Fermi wavevector of the heavy-fermion band (Fig. 1*B* and ref. 7). An intuitive picture of this situation is that the atomic-scale hybridization suppression at the Kondo-hole generates oscillations in $\Delta_h(\mathbf{r}) \propto \delta V_h(\mathbf{r})$ at twice the characteristic wavevector $\mathbf{k}^c(\varepsilon^f)$ of the hybridization process itself (the avoided crossing of the localized f-electron state ε^f and the light prehybridization band $\mathbf{k}^c(\varepsilon)$—see arrow in Fig. 1*B*). Because ε^f is so close to the Fermi level, ε_F, the resulting hybridization oscillation wavevector would be virtually indistinguishable from $2\mathbf{k}_F^c$ and therefore in good agreement with ref. 22. However, no experimental tests of any of these predictions for the electronic structure surrounding a Kondo-hole have been reported.

Spectroscopic Imaging STM

The long term experimental challenges have therefore been: (*i*) to directly visualize the electronic structure of individual Kondo-holes; (*ii*) to image any nanoscale heterogeneity of hybridization generated by random Kondo-hole doping; (*iii*) to determine the alterations to the hybridization strength and thus the heavy-fermion states nearby a Kondo-hole; (*iv*) to search for the states bound within the hybridization gap at each Kondo-hole; and (*v*) to explore the relationship between all these phenomena and the macroscopic transport and thermodynamic observables. In addressing these issues we use SI-STM because it can determine simultaneously the **r**-space and **k**-space electronic structure of correlated electron systems (7–11).

Kondo-Hole Doped Heavy-Fermion System

A canonical example of a Kondo-hole (14) occurs at a spinless Th atom substituted for a magnetic U atom in URu_2Si_2. Despite the incompletely understood "hidden order" phase transition at ~18 K in this material, the observed evolution in **k**-space upon cooling to low temperatures (~2 K) consists of the rapid development of a relatively uncomplicated heavy-fermion system (7, 24, 25). That this is a heavy-fermion metal is well known from specific heat measurements giving $m^* \sim 25\ m_e$ (26) with little change due to thorium dilution (14), as well as from carrier damping in Hall transport data (27), and from quantum oscillations yielding $m^* \sim 30\ m_e$ (28, 29). More directly, angle resolved photoemission studies reveal the expected signature of the **k**-space heavy-fermions—the very slowly dispersing quasiparticle band of f character (24, 25). Even more definitively, heavy quasiparticle interference imaging has visualized directly the splitting of the light conduction band into the two heavy bands and the associated opening of a heavy-fermion hybridization gap (7). These are all as predicted for the appearance of heavy-fermion coherence in a Kondo lattice system (2–4, 30). Collectively, these observations are compelling as to the heavy-fermion character of the **k**-space electronic structure in URu_2Si_2 at low temperatures. Thus, for the purposes of examining the local electronic structure of a Kondo-hole at low temperatures, URu_2Si_2 is effectively a simple heavy-fermion system.

Results

SI-STM Measurements. We use 1% Th-doped URu_2Si_2 samples which are well known to exhibit heavy-fermion phenomena highly similar to those of the nonthorium doped compounds (14). The samples are inserted into the dilution refrigerator based SI-STM system, mechanically cleaved in cryogenic ultrahigh vacuum, and

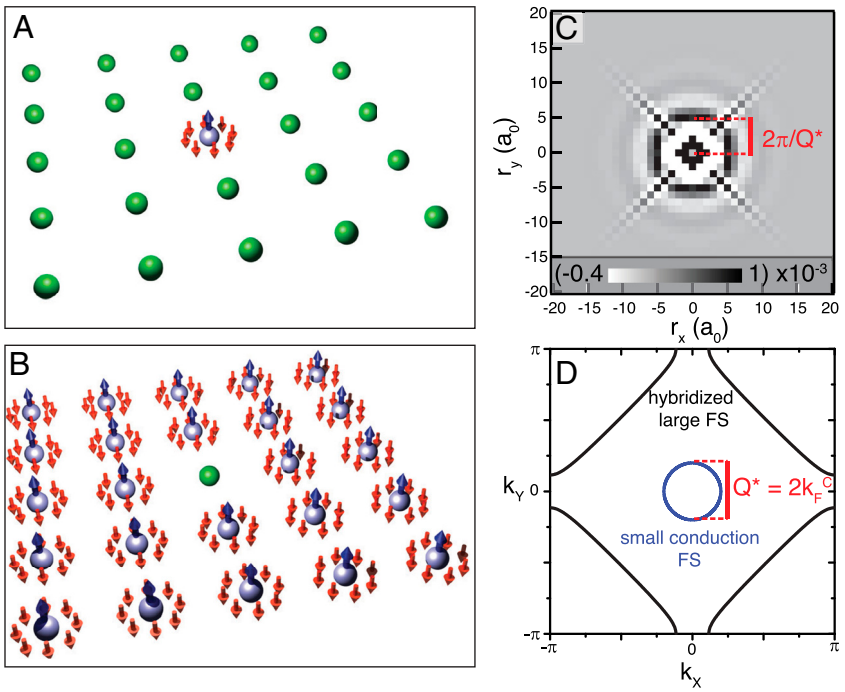

Fig. 2. Theoretical analysis of hybridization oscillations surrounding a Kondo-hole. (*A*) Schematic of a single Kondo resonance. The magnetic atom is shown in blue while the conduction electrons which screen its moment at low temperature are indicated schematically in red. The nonmagnetic atoms in the host metal are green. (*B*) Schematic of a single Kondo-hole. The magnetic atom/spin is shown in blue while the conduction electrons which screen these moments at low temperature are indicated schematically in red. The nonmagnetic atom at the Kondo-hole site is shown in green. (*C*) Theoretical analysis of variations in the intensity of the hybridization strength and thus Δ_h surrounding a Kondo-hole (reproduced with permission from ref. 22). Here the wavevector of strongest perturbation $\mathbf{Q}^*$ is predicted to occur at $\mathbf{Q}^* \cong 2\mathbf{k}_F^\xi$. (*D*) The conduction (small circular) and heavy-fermion bands (large) used in the model of ref. 22 (reproduced with permission). It is obvious by comparison that the hybridization oscillations in Δ_h surrounding the Kondo-hole are predicted to occur at the wavevector $\mathbf{Q}^* \cong 2\mathbf{k}_F^\xi$ and would then be highly distinct from the Friedel oscillation at the heavy-fermion Fermi wavevectors $\mathbf{q} \cong 2\mathbf{k}_F^{HF}$.

then inserted into the STM head. Atomically flat and clean a-b surfaces consisting of layers of U atoms are achieved throughout. Subkelvin ultrahigh vacuum conditions enable long term $g(\mathbf{r},\varepsilon)$ measurements with atomic resolution and register in the same field-of-view (FOV) without any degradation of surface quality. These $g(\mathbf{r},\varepsilon)$ data were acquired with a standard AC lock-in amplifier technique using bias modulations down to 250 μV rms at the lowest temperatures. For **k**-space determination, a FOV of up to 60 nm × 60 nm is used to ensure sufficiently high Fourier resolution in the dispersive scattering interference **q**-vectors (7).

Kondo-Holes and Heavy-Fermion Hybridization. In Fig. 3*A* we show a topographic image of the uranium-termination surface (7) of this material. The location of each Th atom corresponds to an atomic-scale dark dot at sites within the uranium lattice, whose density is in good agreement with the known Th atom density and which are absent in undoped samples. In Fig. 3 *B–D* we show the $g(\varepsilon)$ measured under three different conditions. Fig. 3*B* shows the spatial average of $g(\varepsilon)$ away from Th sites measured above the temperature where the heavy-fermion bands are formed (7, 24, 25). Fig. 3*C* shows the same spatial average $g(\varepsilon)$ measured deep in the heavy-fermion state at 1.9 K but away from Th sites. We see clearly the changes in $g(\varepsilon)$ which are produced by the appearance of the coherent heavy-fermion band structure, and the resulting practical definition of Δ_h as the difference between the energies where $N(\varepsilon)$ departs from its high-temperature values when heavy-fermion bands are absent (green arrows). Fig. 3*D* shows the typical $g(\varepsilon)$ observed at each Th atom as measured at 1.9 K; it always exhibits a quite sharp (δE ~ 1 meV) peak in $N(\varepsilon \sim 0)$. This resonance feature is the long-sought electronic impurity bound-state at a Kondo-hole (19–23).

Hybridization Gapmap. The local hybridization strength in **r**-space is determined by measuring the range of energies between $\Delta_h^-(\boldsymbol{r})$ and $\Delta_h^+(\boldsymbol{r})$ for which $g(\mathbf{r},\varepsilon)$ is distinct from the featureless $g(\mathbf{r},\varepsilon)$ observed before the hybridization-split heavy bands appear (schematically in Fig. 1 *B* and *C*; green arrows in Fig. 3*C* and Fig. 4*C*). To visualize the spatial arrangements of hybridization we therefore introduce the concept of a "hybridization gapmap" $\Delta_h(\mathbf{r}) = \Delta_h^+(\mathbf{r}) - \Delta_h^-(\mathbf{r})$ for heavy-fermion compounds [by analogy to the "superconducting gapmap" technique (31)]. Recall that this corresponds closely to the theoretical definition (4) of $\Delta_h(\mathbf{r})$ i.e., the difference between the energies of the heavy-fermion bands $\varepsilon^-(\mathbf{k})$ and $\varepsilon^+(\mathbf{k})$ measured at $\mathbf{k}^c(\varepsilon^f)$ (Fig. 1*B*). A typical result for $\Delta_h(\mathbf{r})$ in a 40 × 40 nm square FOV is shown in Fig. 3*E* (topograph in *SI Text*). The hybridization strength is highly heterogeneous at the nanoscale ranging in energy over ~5 mV. The inset shows how the hybridization oscillations are actually centered on the Th atoms. The unexpectedly intense and widespread hybridization disorder (Fig. 3*E*) then stems from the long-range nature of these hybridization oscillations in combination with the randomness of the Th sites upon which they are centered. Although hybridization disorder has long been anticipated for randomly Kondo-hole doped heavy-fermion systems (12–16, 19–23) it is compelling to observe it directly and to understand its origin and intensity in terms of long-range hybridization oscillations.

Discussion and Conclusions

Fourier analysis of hybridization gapmaps in Th-doped URu_2Si_2 (e.g., Fig. 3*E*) reveals that the apparently complex fluctuations in $\Delta_h(\mathbf{r})$ actually contain a quite simple structure. The Fourier transform, $\Delta_h(\mathbf{q})$, of $\Delta_h(\mathbf{r})$ from Fig. 3*E* is shown in Fig. 4*A* (see *SI Text*). Here we see that the hybridization strength is modulating in space with a characteristic wave vector $\mathbf{Q}^*$ as identified by the arrow. This observation can be compared with

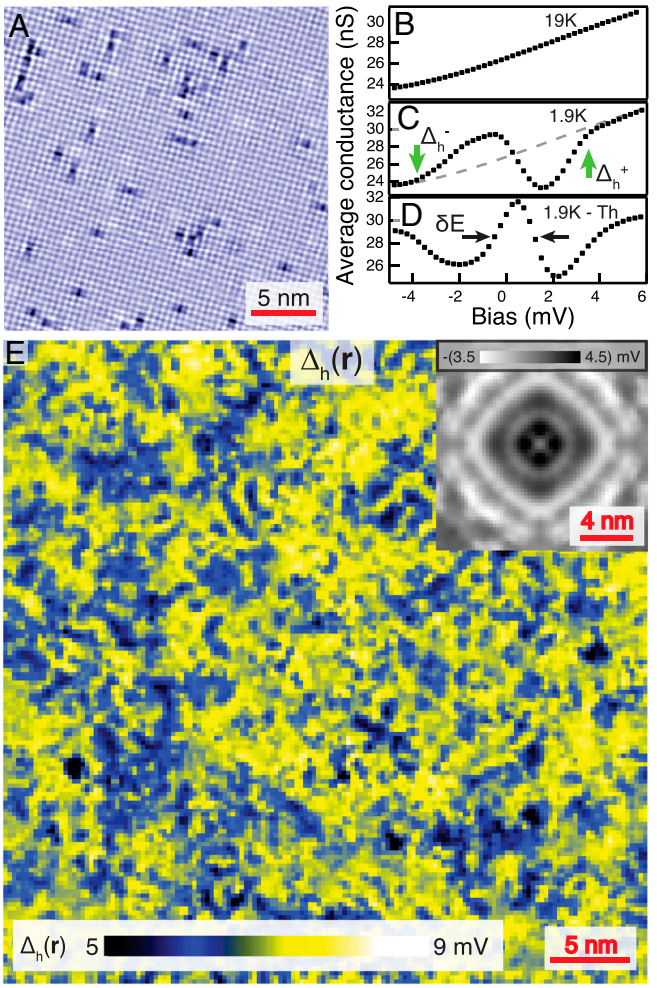

Fig. 3. Visualization of the effect of Kondo-holes on the **r**-space hybridization strength. (*A*) Topographic image of the uranium-terminated (7) surface of URu_2Si_2. The locations of the Th atoms substituted on the U sites appear as dark dots whose density is in agreement with the 1% substitution level. The image has been Fourier filtered to more clearly reveal the position of the Th atoms of the U lattice. (*B*) The tunneling spectrum $g(\varepsilon)$ far from the Th sites when measured at $T \sim 19$ K well above the temperature where the heavy-fermion bands are observed to form. (*C*) The tunneling spectrum $g(\varepsilon)$ measured at $T \sim 2$ K after the heavy-fermion bands have become established (7) and far from the Th sites. The magnitude of the hybridization gap Δ_h can be determined by identification of the energy range where $g(\varepsilon)$ has been perturbed due to the *HF* band structure as shown by vertical green arrows (see Fig. 1 *B* and *C*). (*D*) The tunneling spectrum $g(\varepsilon)$ measured at $T \sim 2$ K at representative Th atom sites. Here the changes in hybridization can be determined from the energy range where $g(\varepsilon)$ is perturbed. The new local electronic state bound within the hybridization gap at each Th-atom Kondo-hole site is seen as a sharp peak in $g(\varepsilon)$ near $\varepsilon \sim 0$. (*E*) The heavy-fermion hybridization gapmap shows the spatial variations in hybridization strength as indicated by the color scale shown in the inset. The image is a direct visualization of nanoscale spatial variations of the hybridization energy $\Delta_h(\mathbf{r})$ in a Kondo-hole doped heavy-fermion compound. The inset shows directly how the hybridization oscillations are actually centered on the Th sites; it is the average of the lower hybridization gap edge $\Delta_h^-(\mathbf{r})$ (because this exhibits the highest contrast) over all locations centered on a thorium atom.

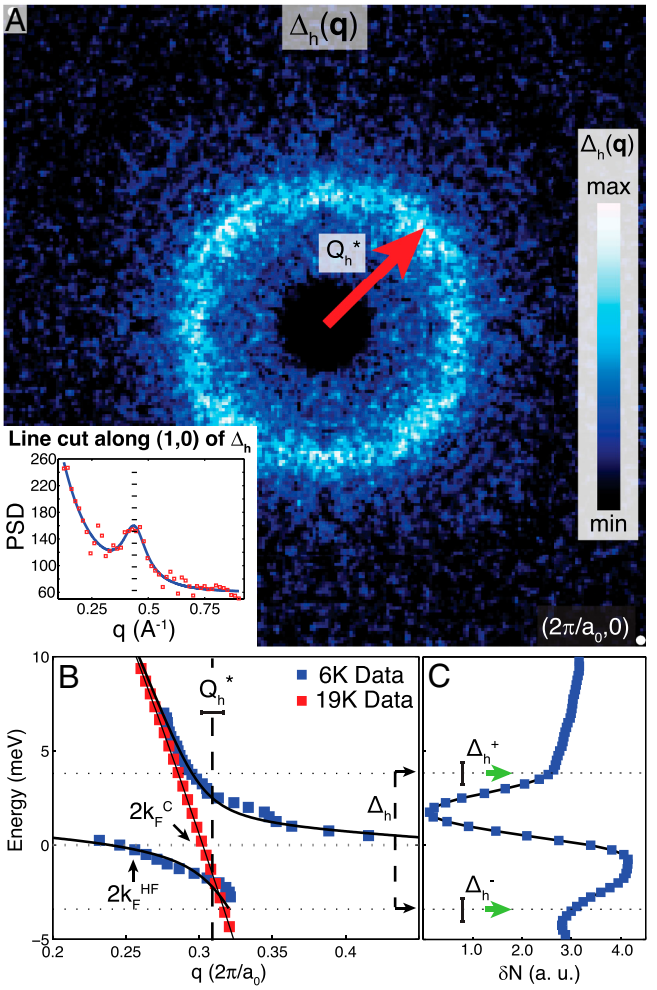

Fig. 4. Structure of hybridization oscillations in **q**-space. (*A*) The Fourier transform of data in Fig. 3*E* revealing that the perturbations to hybridization in a random distribution of Kondo-holes are not completely random because of the hybridization oscillations surrounding each Th atom. The central peak of the Fourier transform which is generated by the randomness of Th dopant disorder has been removed for clarity. An example of the measured wavevector of the hybridization oscillations $\mathbf{Q}^*$ is shown by the red arrow. The four dots in the corner of the image occur at values of $\mathbf{q} = (0,2\pi/a_0)$; $(2\pi/a_0,0)$ where a_0 is the unit cell dimension. The inset shows the quantitative measurement of $\mathbf{Q}^*$. (*B*) The measured characteristics of the light conduction band $\mathbf{k}^c(\varepsilon)$ observed above the temperature of heavy-fermion formation, with its Fermi wavevector $\mathbf{k}_F^c(\varepsilon)$ are shown in red. In blue, the characteristics, measured using heavy quasiparticle interference (7), of the two heavy bands which are formed from the light conduction band by the avoided crossing. Here the heavy-fermion Fermi wavevector is $\mathbf{k}_F^{HF}(\varepsilon)$. The theoretical definition (4) of Δ_h for heavy-fermion bands $\mathbf{k}_\pm^c(\varepsilon)$ is shown by the horizontal dotted lines. The measured wavevector of the hybridization oscillations $\mathbf{Q}^*$ is shown by a vertical dashed line. (*C*) The associated changes in conductance $\delta g(\varepsilon)$ measured by subtracting the $g(\varepsilon)$ at low temperature from that at high temperature. The plot shows how the evaluation in **r**-space of Δ_h is carried out using the difference in energy between the energies Δ^+ and Δ^- where $g(\varepsilon)$ departs from its value before heavy-fermion formation (green arrows). (The plot also shows that Δ_h measured independently in this fashion is in very good agreement with that measured in **k**-space).

the theoretical predictions from Fig. 2*C* (22) that hybridization modulations should exist at each Kondo-hole. In Fig. 4 *B* and *C* we show the heavy-fermion band structure of this material measured using quasiparticle interference imaging (7), along with associated changes in $N(\varepsilon)$. This simple **k**-space structure is in excellent agreement with basic heavy-fermion theory (3–5). Fig. 4*C*, which uses the same vertical axis as Fig. 4*B*, shows the energy range Δ_h in which the changes in the $g(\varepsilon)$ due to hybridization are observed. This comparison is highly consistent with theoretical expectations for the relationship between **k**-space and **r**-space electronic structure of a heavy-fermion compound (Fig. 1 *B* and *C*). The inset to Fig. 4*A* is the power spectral density measured along a typical radius in Fig. 4*A* showing that the oscillations of hybridization strength occur at the wavevector $|\mathbf{Q}^*| = 0.3 \pm 0.01$ $(2\pi/a_0)$ in good agreement with the **r**-space hybridiza-

tion periodicity observed surrounding the Th sites (Fig. 3*E* inset). The oscillation wavevector is identified by the vertical dashed line in Fig. 4*B* thereby revealing that the hybridization oscillations occur at $\mathbf{Q}\cong 2\mathbf{k}_F^c$ (arrow) very close to where the light conduction band avoids its crossing with ϵ^f and quite inconsistent with $\mathbf{Q}\cong 2\mathbf{k}_F^{HF}$ (arrow).

Long-standing theoretical predictions (19–23) for the electronic structure of a Kondo-hole including the suppression of hybridization near the substitution-atom sites (Fig. 3*D*), the disordered hybridization fluctuations generated by random Kondo-hole doping (Fig. 3*E*), that an impurity bound-state appears within the hybridization gap (Fig. 3*D*) and that hybridization oscillations exist and exhibit $\mathbf{Q}\cong 2\mathbf{k}_F^c$ (Fig. 4*A*) are borne out directly by these experiments. This agreement between theory (19–23), deductions from macroscopic experiments (12–18), and our observations at spinless Th atoms makes it highly implausible that these effects stem from another mechanism and, conversely, provides growing confidence in the ability to predict theoretically and to detect experimentally the atomic-scale electronic structure and, perhaps more importantly, the consequent hybridization disorder generated by Kondo-holes. Future work will seek to establish any specific effects of the hidden order in URu_2Si_2 on the Kondo-hole electronic structure and the universal characteristics of Kondo-holes in a variety of other heavy-fermion systems. Nevertheless, the advances we report here will be consequential for studies of nanoscale hybridization heterogeneity, local perturbations to heavy-fermion formation, Kondo-hole bound states, and suppression of coherence and superconductivity in Kondo-hole doped heavy-fermion systems. The combination of SI-STM techniques introduced here and in ref. 7 also provide a powerful approach for study of the **r**-space and **k**-space electronic structure of heavy-fermion systems.

ACKNOWLEDGMENTS. We thank P. Coleman, P. Chandra, T. Durakievich, J. Figgins, Z. Fisk, M. Graf, K. Haule, E.-A. Kim, G. Kotliar, D.-H. Lee, D. Morr, K.M. Shen, F. Steglich, Z. Tešanović, J. Thompson, M. Vojta, and J.X. Zhu, for helpful discussions and communications. These studies at Brookhaven National Laboratory and Cornell University were supported by the Department of Energy, Office of Basic Energy Sciences. Research at McMaster was supported by National Science and Engineering Research Council of Canada and Canadian Institute for Advanced Research. Research at Los Alamos was supported by the Department of Energy Office of Basic Energy Sciences, Materials Sciences Division, and in part by the Center for Integrated Nanotechnology, a Department of Energy Office of Basic Energy Sciences user facility, under contract DE-AC52-06NA25396. I.A.F. acknowledges support from Fundação para a Ciência e a Tecnologia, Portugal under fellowship number SFRH/BD/60952/2009.

1. Doniach S (1977) The Kondo lattice and weak antiferromagnetism. *Physica B* 91:231–234.
2. Hewson AC (1993) *The Kondo Problem to Heavy Fermions* (Cambridge University Press, Cambridge).
3. Steglich F (2005) Superconductivity and magnetism in heavy fermion compounds. *J Phys Soc Jpn* 74:167–177.
4. Coleman P (2007) *Handbook of Magnetism and Advanced Magnetic Materials Volume Fundamental Theory*, eds H Kronmüller and S Parkin (Wiley and Sons, New York), pp 95–148.
5. Maltseva M, Dzero M, Coleman P (2009) Electron cotunneling into a Kondo lattice. *Phys Rev Lett* 103:206402.
6. Figgins J, Morr DK (2010) Differential conductance and quantum interference in Kondo systems. *Phys Rev Lett* 104:187202.
7. Schmidt AR, et al. (2010) Imaging the Fano lattice to 'hidden order' transition in URu_2Si_2. *Nature* 465:570–576.
8. Ernst S, et al. (2011) Emerging local quantum entanglement and heavy fermion formation within the Kondo lattice of $YbRh_2Si_2$. *Nature* 474:362–366.
9. Madhavan V, et al. (1998) Tunneling into a single magnetic atom: spectroscopic evidence of the Kondo resonance. *Science* 280:567–569.
10. Manoharan H, Lutz C, Eigler D (2000) Quantum mirages formed by coherent projection of electronic structure. *Nature* 403:512–515.
11. Knorr N, et al. (2002) Kondo effect in single Co adatoms on Cu surfaces. *Phys Rev Lett* 88:096804.
12. Steglich F, et al. (1987) Heavy fermions and superconductivity: "superconducting spectroscopy" of non-magnetic impurities in $CeCu_2Si_2$. *Physica B* 148:6–13.
13. Lin C, et al. (1987) Heavy-fermion behavior and the single-ion Kondo model. *Phys Rev Lett* 58:1232–1235.
14. Lopez A, et al. (1992) Th-doped URu_2Si_2: influence of Kondo holes on coexisting superconductivity and magnetism. *Physica B* 179:208–214.
15. Lawrence JM, et al. (1996) Kondo hole behavior in $Ce_{0.97}La_{0.03}Pd_3$. *Phys Rev B* 53:12559–12562.
16. Petrovic C, et al. (2002) Effects of La substitution on the superconducting state of $CeCoIn_5$. *Phys Rev B* 66:054534.
17. Paglione J, et al. (2007) Incoherent non-Fermi liquid scattering in a Kondo lattice. *Nature Phys* 3:703–706.
18. Bauer ED, et al. (2011) Electronic inhomogeneity in a Kondo lattice. *Proc Natl Acad Sci USA* 108:6857–6861.
19. Tešanovic Z (1986) Disorder and coherence in heavy fermion systems. *Phys Rev B* 34:5212–5216.
20. Sollie R, Schlottmann P (1991) A simple theory of the Kondo hole. *J Appl Phys* 69:5478–5480.
21. Sollie R, Schlottmann P (1991) Local density of states in the vicinity of a Kondo hole. *J Appl Phys* 70:5803–5805.
22. Figgins J, Morr DK (2011) Defects in heavy-fermion materials: unveiling strong correlations in real space. *Phys Rev Lett* 107:066401.
23. Hirschfeld P, Vollhardt D, Wölfle P (1986) Resonant impurity scattering in heavy fermion superconductors. *Solid State Commun* 59:111–115.
24. Santander-Syro AF, et al. (2009) Fermi-surface instability at the 'hidden-order' transition of URu_2Si_2. *Nature Phys* 5:637–641.
25. Yoshida R, et al. (2010) Signature of hidden order and evidence for periodicity modification in URu_2Si_2. *Phys Rev B* 82:205108.
26. Maple MB, et al. (1986) Partially gapped Fermi surface in the heavy-electron superconductor URu_2Si_2. *Phys Rev Lett* 56:185–188.
27. Schoenes J, Schönenberger C, Franse J (1987) Hall effect and resistivity study of the heavy-fermion system URu_2Si_2. *Phys Rev B* 35:5375–5378.
28. Ohkuni H, et al. (1999) Fermi surface properties and the de Haas-van Alphen oscillation in both the normal and superconducting mixed states of URu_2Si_2. *Philos Mag B* 79:1045–1077.
29. Hassinger E, et al. (2010) Similarity of the Fermi surface in the hidden order state and the antiferromagnetic state of URu_2Si_2. *Phys Rev Lett* 105:216409.
30. Yuan T, Figgins J, Morr DK (2011) Hidden order transition in URu_2Si_2 and the emergence of a coherent Kondo lattice., arXiv:1101.2636v1.
31. Lang KM, et al. (2002) Imaging the granular structure of hight-T_c superconductivity in underdoped $Bi_2Sr_2CaCu_2O_{8+\delta}$. *Nature* 415:412–416.